J. Shanghai Jiao Tong Univ. (Sci.), 2022
https://doi.org/10.1007/s12204-022-2551-1

Dynamic Train Vertical Sperling Index Evaluation Model Considering Wheel-Rail Contact Loss

LIU Yiling[1] (刘怡伶), *ZHANG Jingwei*[1] (张经纬), *LIU Xuewen*[1*] (刘学文),
WANG Yansong[1] (王岩松), *ZHOU Yueting*[2] (周跃亭)
(1. School of Mechanical and Automotive Engineering, Shanghai University of Engineering Science, Shanghai 201620, China; 2. School of Aerospace Engineering and Applied Mechanics, Tongji University, Shanghai 200092, China)

Abstract: In this study, a half-space 13-degree-of-freedom vehicle model, a double track model, and a train-bridge interaction model were integrated to form a combined people-train-rail-bridge interaction model to analyze the vertical Sperling index of the train body and passengers as realistically as possible. In this bigger, more complete, and novel model, the separation between the vehicle and bridge is considered. By comparing measured data and simulated results obtained using the proposed model with the Newmark-Beta algorithm, the effectiveness of the model was verified, and the results demonstrated that these two values were very close. Upon further numerical analysis, the dynamic responses of the train and the three equivalent human bodies at different train speeds were computed using the developed vehicle-structure dynamic analysis program with different abruptness values in the random rail irregularities. The results of these four dynamic responses revealed that the rail irregularities affected the vertical acceleration of the three equivalent human bodies and train, and the best Sperling index evaluation standard for the train was not fixed (as assumed when only considering the train body) but varied with the passenger position as the train traveled over irregularities.
Key words: equivalent mechanical model, people-train-rail-bridge interaction, Sperling index analysis, mass-spring-damping theory
CLC number: U 270 **Document code:** A

0 Introduction

Rail transportation is crucial for urban development. Improvements in its convenience and comfort are directly related to the market status of rail transit[1]. Passenger comfort due to the vehicle-line-viaduct coupling vibrations is thus important in the design of bridges, trains, and even the seats on the trains[2], and the Sperling index is important for comfort evaluation.

Numerous studies of vehicle-road and vehicle-bridge interactions have been conducted, such as those by Yang et al.[3-4], Frýba[5], Xiao et al.[6], Hung and Hsu[7], and Ling et al[8]. Most of these studies considered the riding comfort as the train passed over a viaduct. The riding comfort of a vehicle is significantly affected by the vertical acceleration response[9]. Many researchers have analyzed the riding comfort with respect to the vehicle body[10-11], automotive seats[12], or road irregularities[13] based on the classical vehicle model. Youcef et al.[14] combined a 10-degree-of-freedom (10-DOF) vehicle model with a simply supported beam to form a simple vehicle-bridge interaction model and then used the modal superposition method to analyze the vibration responses of the bridge body, comfort, and other factors that have a significant impact on the interactions due to various rail irregularities. There have also been many examples of flexural vibrations of the railway vehicle bodies, such as Tomioka et al.[15-17], Hui et al.[18], Gong et al.[19], and Dumitriu[20]. For comfort and train bending vibration problems, Dumitriu[21] introduced a new passive approach to improve the vehicle ride comfort. This approach limited the rotation of the vehicle body by fixing two anti-bending bars onto the longitudinal beams of the 10-DOF train model under the frame. However, there are two shortcomings of these models: the wheels and the rail are always assumed to be in contact during the operation of the train; the passenger riding comfort is not considered in the passenger-vehicle-line-bridge interaction system.

During the operation of the train, there will be a

Received: 2021-07-02 **Accepted:** 2021-11-10
Foundation item: the National Natural Science Foundation of China (Nos. 51675324, 11972257 and 11832014), the Project of the Science and Technology Commission of Shanghai Municipality (No. 19030501100), and the Technical Service Platform for Vibration and Noise Testing and Control of New Energy Vehicles (No. 18DZ2295900)
∗**E-mail:** xuewen2018@126.com

wheel jumping state, which is a state between the wheel-rail contact and derailment[22]. Liu et al.[23] proposed a semi-analytical solution method to study the wheel jumping conditions, established a double-track-bridge model, and combined it with the classic 10-DOF vehicle model to calculate the vibration responses of a vehicle, floating slab, rail, and bridge. There have been few reports that include both features mentioned above.

Indicators of riding comfort are often determined by the vehicle body's vibration response. Previous reports[24-25] point out that the train comfort criterion is that the maximum vertical acceleration was less than 0.49 m/s^2. The Eurocode[26] states that the train's comfort criterion is that the maximum vertical acceleration is less than 1.0 m/s^2. According to China's Railway Vehicles Specification, during the evaluation of the dynamic performance and accreditation tests, the train comfort criterion is that the maximum vertical acceleration is less than 2.5 m/s^2. In recent years, with the stricter requirements, the study of riding comfort has begun to focus on the development of quantitative evaluation methods[27].

Based on the classic 10-DOF model and single Euler beam, a more integrated and realistic passenger-vehicle-line-viaduct model was established in this study. The alterable element method[28] and equivalent human body model are used in the new model, and the dynamic changes of wheel-rail contact states are considered to calculate the dynamic responses of the equivalent humans and vehicle body for different speeds and rail irregularities. Finally, the Sperling index, based on the vehicle body and passenger dynamics, is explored.

1 Mechanical Human-Train Model

Figure 1 shows the mechanical model of a four-wheel, two-suspension vehicle, coupled with three equivalent passenger masses, which are distributed at three points (one at the midpoint of the vehicle body, and two at side points, where the vehicle body and the bogies are coupled). The train travels on a viaduct at a constant speed with rail irregularities, and the dynamic responses are described via the functions presented in Section 2.

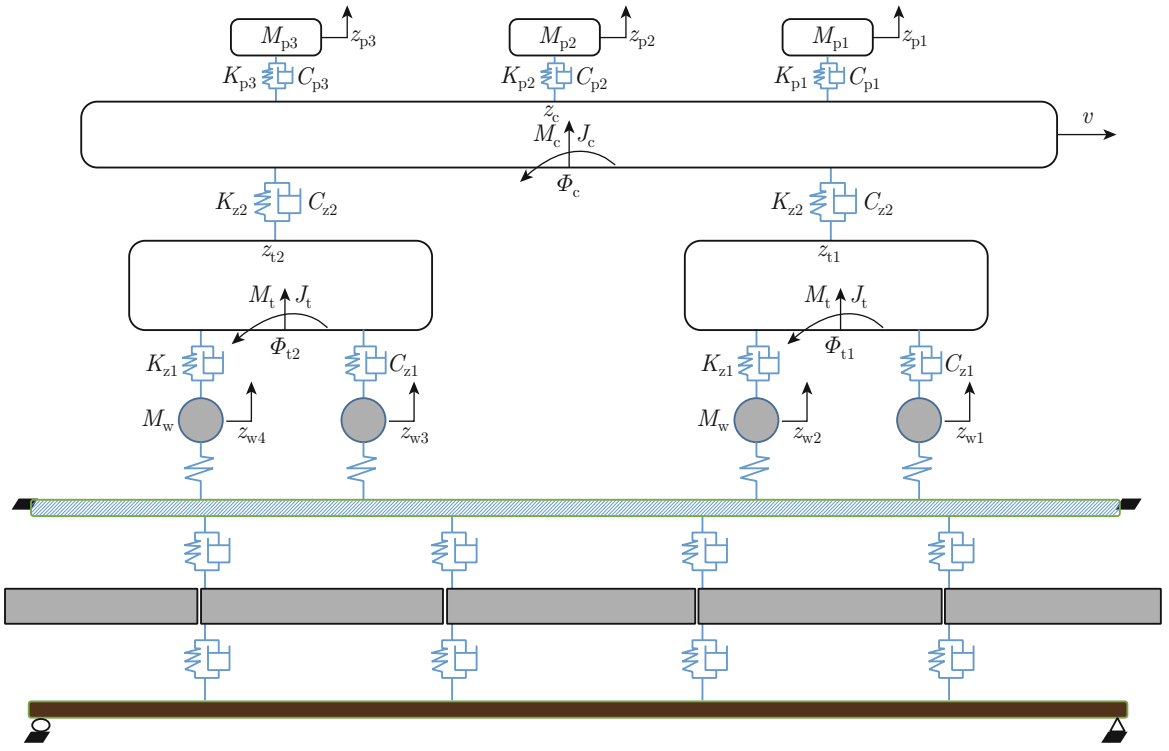

Fig. 1 Half space 13-DOF human-train line interaction model

The classical 10-DOF model consists of a vehicle body with mass of M_c, two bogies with mass of M_t, and four wheels with mass of M_w. For the vehicle-body, the vertical displacement z_c and pitching motion Φ_c are considered, and the moment of inertia of the vehicle-body is denoted as J_c. For the bogies, the vertical displacements z_{ti} (i = 1, 2) and pitching motion Φ_{ti} (i = 1, 2) are considered, where i denotes the ith bogie, and the moment of inertia of the bogies is J_t. For the wheels, only vertical displacements z_{wi} (i = 1, 2, 3, 4) are considered, where i denotes the ith wheel. The wheels and bogies are connected by primary

suspension spring and damper, which are denoted as K_{z1} and C_{z1} respectively. The bogies and vehicle-body are connected by secondary suspension spring and damper, which are denoted as K_{z2} and C_{z2} respectively. The mass of a single passenger is miniscule relative to the mass of the vehicle in the model, and thus, accurate calculations for the individual passengers cannot be carried out. In this paper, all of the passengers in the coach are represented as three masses, which are distributed at two points where the vehicle body and the bogies are coupled and at the midpoint of the vehicle body. Extra points of the entire carriage can be obtained by interpolation using the values at these three points.

The model in this paper is built based on the following assumptions:

(1) Only vertical vibrations are considered.

(2) A 10-DOF rigid body model is adopted for the vehicle.

(3) The length of one span of a simply supported bridge is l_b, and two roughness conditions of the pavement are considered: the bridge roughness and zero roughness when the train is not traveling over the bridge.

(4) The vehicle speed is constant.

(5) The longitudinal forces between the vehicles are equal.

(6) The transient jump of the wheel is considered.

(7) The number of carriage occupants is 99, and the average mass of each passenger is 75 kg. With the lumped-mass method, all of the passengers in the coach are equivalent to three equivalent rigid mass blocks M_{pi}, where i denotes the ith rigid mass block. The three equivalent human bodies only have one DOF, z_{pi} (i = 1, 2, 3) are vertical displacements, and their stiffness and damping are denoted as K_{pi} and C_{pi} (i = 1, 2, 3), respectively.

2 Equation of Motion

The direct cause of the human-train and track-bridge interactions is the vibration deformation of the wheelset and rail, which causes wheel-rail contact deformation and a change of the contact geometry. Therefore, determining the relationship between the wheel and rail is the first step for determining the vibration equation of the interaction model.

The equations of equilibrium of the wheelsets are given as

$$M_{w1}\ddot{z}_{w1} = M_{w1}g + F_{tw1} - p_1, \tag{1}$$

$$M_{w2}\ddot{z}_{w2} = M_{w2}g + F_{tw2} - p_2, \tag{2}$$

$$M_{w3}\ddot{z}_{w3} = M_{w3}g + F_{tw3} - p_3, \tag{3}$$

$$M_{w4}\ddot{z}_{w4} = M_{w4}g + F_{tw4} - p_4, \tag{4}$$

where M_{wi} is the mass of wheels, z_{wi} is vertical displacements, g is the acceration of gravity, F_{twi} denotes the interaction force between bogie and wheel set, and p_i denotes the coupling forces between wheels and rail (i = 1, 2, 3, 4, i denotes the ith wheel). The coupling forces between the wheel and rails are expressed as

$$p_i = K_h(z_{wi} - z_b(x,t)|_{x=vt} + A_{Irr}), \tag{5}$$

where $z_b(x,t)|_{x=vt}$ is the vertical displacement of the rail below the ith wheel at the time t, and v is train speed, A_{Irr} is the abruptness of the irregularity at that location, and K_h denotes the coupling stiffness between the wheels and rail:

$$K_h = \begin{cases} K_h, & \text{the spring is condensed} \\ 0, & \text{the spring is pulled long} \end{cases}. \tag{6}$$

2.1 Human-Train Model

The equivalent passenger model consists of three rigid mass blocks, as shown in Fig. 2, where l_c is the distance between two adjacent equivalent human-body mass points, F_{cp1}, F_{cp2}, and F_{cp3} denote the forces loaded on the equivalent human body at the front, middle, and rear coupling points, respectively.

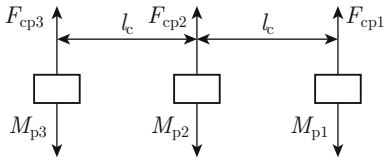

Fig. 2 Equivalent human force diagram

The equilibrium equations of the equivalent human model can be expressed as

$$F_{cp1} = K_{p1}(z_{p1} - z_c + l_c\Phi_c) + C_{p1}(\dot{z}_{p1} - \dot{z}_c + l_c\dot{\Phi}_c), \tag{7}$$

$$F_{cp2} = K_{p2}(z_{p2} - z_c) + C_{p2}(\dot{z}_{p2} - \dot{z}_c), \tag{8}$$

$$F_{cp3} = K_{p3}(z_{p3} - z_c - l_c\Phi_c) + C_{p3}(\dot{z}_{p3} - \dot{z}_c - l_c\dot{\Phi}_c). \tag{9}$$

All of the passengers in the coach are divided into three equal parts. Therefore, the stiffness coefficients, damping coefficients, and mass of these three parts are expressed as

$$K_{p1} = K_{p2} = K_{p3},$$
$$C_{p1} = C_{p2} = C_{p3},$$
$$M_{p1} = M_{p2} = M_{p3}.$$

The vibration equations of the human equivalent model can be expressed as

$$M_{p1}\ddot{z}_{p1} = M_{p1}g - F_{cp1}, \tag{10}$$

$$M_{p2}\ddot{z}_{p2} = M_{p2}g - F_{cp2}, \tag{11}$$

$$M_{p3}\ddot{z}_{p3} = M_{p3}g - F_{cp3}. \tag{12}$$

In the classical half-space 10-DOF vehicle vibration equation[22], the human-train-viaduct model with 13-DOF can be expressed as

$$\boldsymbol{M}_{\mathrm{v}}\ddot{\boldsymbol{u}}_{\mathrm{v}}+\boldsymbol{C}_{\mathrm{v}}\dot{\boldsymbol{u}}_{\mathrm{v}}+\boldsymbol{K}_{\mathrm{v}}\boldsymbol{u}_{\mathrm{v}}=\boldsymbol{Q}_{\mathrm{v}}, \tag{13}$$

where $\boldsymbol{u}_{\mathrm{v}}$, $\boldsymbol{M}_{\mathrm{v}}$, $\boldsymbol{C}_{\mathrm{v}}$, and $\boldsymbol{K}_{\mathrm{v}}$ are the generalized displacement vector, mass matrix, damping matrix, and stiffness matrix, respectively. The generalized force vector $\boldsymbol{Q}_{\mathrm{v}}$ is expressed as

$$\begin{aligned}\boldsymbol{Q}_{\mathrm{v}}=&[0\ \ 0\ \ 0\ \ 0\ \ 0\ \ 0\ \ aM_{\mathrm{w1}}g-F_1\ \ aM_{\mathrm{w2}}g-F_2\\&aM_{\mathrm{w3}}g-F_3\ \ aM_{\mathrm{w4}}g-F_4\ \ 0\ \ 0\ \ 0],\end{aligned} \tag{14}$$

where F_1, F_2, F_3, F_4 denote the coupling forces between wheel set and rail, the spring connection model is used to connect the wheelset and the rail, and the wheel rail separation state is considered:

$$a=\begin{cases}1, & \text{jump}\\ 0, & \text{no jump}\end{cases}. \tag{15}$$

The generalized displacement vector is

$$\begin{aligned}\boldsymbol{u}_{\mathrm{v}}=&[z_{\mathrm{c}}\ \ \varPhi_{\mathrm{c}}\ \ z_{\mathrm{t1}}\ \ \varPhi_{\mathrm{t1}}\ \ z_{\mathrm{t2}}\ \ \varPhi_{\mathrm{t2}}\ \ z_{\mathrm{w1}}\ \ z_{\mathrm{w2}}\ \ z_{\mathrm{w3}}\\&z_{\mathrm{w4}}\ \ z_{\mathrm{p1}}\ \ z_{\mathrm{p2}}\ \ z_{\mathrm{p3}}].\end{aligned} \tag{16}$$

The generalized velocity vector is

$$\begin{aligned}\dot{\boldsymbol{u}}_{\mathrm{v}}=&[\dot{z}_{\mathrm{c}}\ \ \dot{\varPhi}_{\mathrm{c}}\ \ \dot{z}_{\mathrm{t1}}\ \ \dot{\varPhi}_{\mathrm{t1}}\ \ \dot{z}_{\mathrm{t2}}\ \ \dot{\varPhi}_{\mathrm{t2}}\ \ \dot{z}_{\mathrm{w1}}\ \ \dot{z}_{\mathrm{w2}}\ \ \dot{z}_{\mathrm{w3}}\\&\dot{z}_{\mathrm{w4}}\ \ \dot{z}_{\mathrm{p1}}\ \ \dot{z}_{\mathrm{p2}}\ \ \dot{z}_{\mathrm{p3}}].\end{aligned} \tag{17}$$

The generalized acceleration vector is

$$\begin{aligned}\ddot{\boldsymbol{u}}_{\mathrm{v}}=&[\ddot{z}_{\mathrm{c}}\ \ \ddot{\varPhi}_{\mathrm{c}}\ \ \ddot{z}_{\mathrm{t1}}\ \ \ddot{\varPhi}_{\mathrm{t1}}\ \ \ddot{z}_{\mathrm{t2}}\ \ \ddot{\varPhi}_{\mathrm{t2}}\ \ \ddot{z}_{\mathrm{w1}}\ \ \ddot{z}_{\mathrm{w2}}\ \ \ddot{z}_{\mathrm{w3}}\\&\ddot{z}_{\mathrm{w4}}\ \ \ddot{z}_{\mathrm{p1}}\ \ \ddot{z}_{\mathrm{p2}}\ \ \ddot{z}_{\mathrm{p3}}].\end{aligned} \tag{18}$$

The generalized mass matrix is

$$\begin{aligned}\boldsymbol{M}_{\mathrm{v}}=&\mathrm{diag}(M_{\mathrm{c}},J_{\mathrm{c}},M_{\mathrm{t}},J_{\mathrm{t}},M_{\mathrm{t}},J_{\mathrm{t}},M_{\mathrm{w1}},M_{\mathrm{w2}},M_{\mathrm{w3}},\\&M_{\mathrm{w4}},M_{\mathrm{p1}},M_{\mathrm{p2}},M_{\mathrm{p3}}).\end{aligned} \tag{19}$$

The $\boldsymbol{C}_{\mathrm{v}}$ and $\boldsymbol{K}_{\mathrm{v}}$ parameters of the vehicle body in this 13-DOF model matrix are provided in Appendix A.

2.2 Track and Viaduct Model

In the analysis model, the structure of the track-viaduct system is not a single simply supported beam but a double-layer vibration model that includes the rail. The floating slabs, viaduct, and rail were simulated as an Euler beam, while the floating slab was simulated as a rigid mass structure. The vibration equations and the parameter of the track and viaduct model are presented in Appendix B.

2.3 Analysis of Wheels Jump

This study focuses on the riding comfort of the vehicle and passengers under the condition that wheels and tracks will be separated. The model of the wheel's jump and the status of the spring at different phases are shown in Fig. 3. Line 1 indicates the initial phase of the spring. Line 2 indicates the static equilibrium status of the spring, and the circled numbers indicate the different jump phases of the spring. The vehicle wheel and the bridge experience different forces when the contact spring is at different states, as shown in Table 1, where $G=(M_{\mathrm{c}}+2M_{\mathrm{t}}+4M_{\mathrm{w}})g$, and $\varDelta$ is the amount of compression between the wheel and the structure.

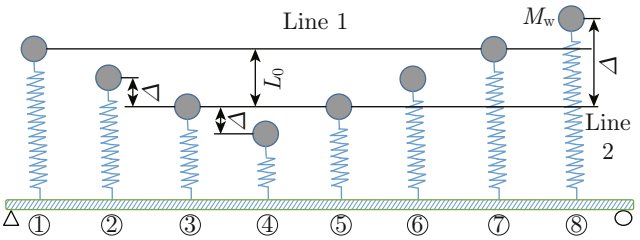

Fig. 3 Different states of moving wheel jumping from bridge

Table 1 Force acting on vehicle and bridge at different states

State number	Compression value	Force on wheel	Force on bridge
①	$\varDelta=-L_0$	$M_{\mathrm{w}}g$	0
②	$-L_0<\varDelta<0$	$-K_{\mathrm{h}}\varDelta$	$(G/4+K_{\mathrm{h}}\varDelta)$
③	$\varDelta=0$	0	$M_{\mathrm{w}}g$
④	$\varDelta>0$	$-K_{\mathrm{h}}\varDelta$	$(G/4+K_{\mathrm{h}}\varDelta)$
⑤	$\varDelta=0$	0	$M_{\mathrm{w}}g$
⑥	$-L_0<\varDelta<0$	$-K_{\mathrm{h}}\varDelta$	$(G/4+K_{\mathrm{h}}\varDelta)$
⑦	$\varDelta=-L_0$	$M_{\mathrm{w}}g$	0
⑧	$\varDelta<-L_0$	$M_{\mathrm{w}}g$	0

3 Program Algorithms

The Newmark-Beta method with parameters $\gamma=0.505$ and $\beta=0.252\,506\,25$ was used to solve the equations of motion. The flow-chart of semi-analytical solution method is shown in Fig. 4[22]. Using the model and solution process, the vehicle-structure dynamic analysis program (VSDAP), which is a console application, was then coded in Fortran.

4 Model Validation

The vibrations of Shanghai Metro Line 5 were measured in the field. The measurements were performed on the Xinmin line, 320 m west of the Yindu Road

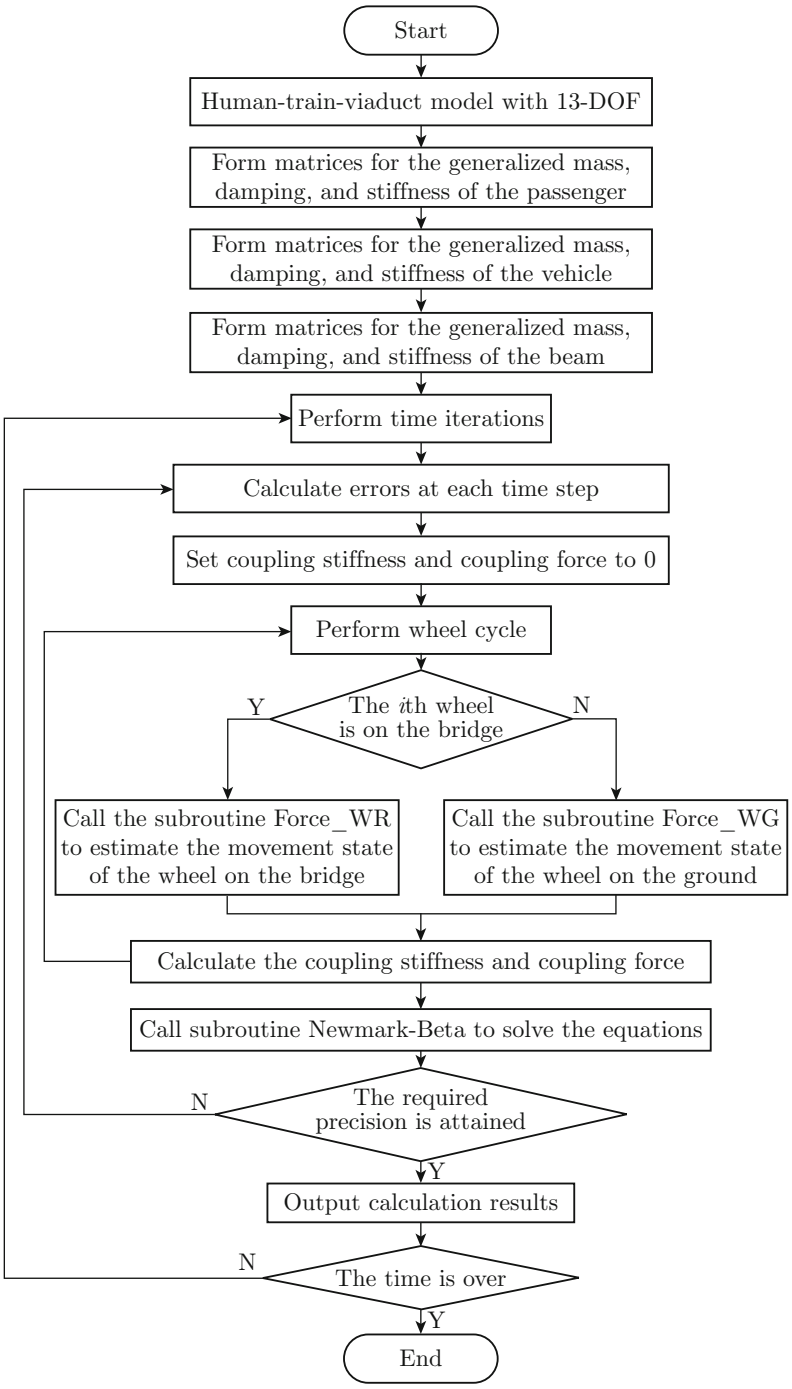

Fig. 4 Flow-chart of semi-analytical solution method

Station. To ensure that the measured train data was consistent with the model proposed in this paper, the spring stiffness and damping of the bearing under the floating slab were set to be very large and zero, respectively, to simulate the directly connected structure between the bearing block and viaduct in the subway line. For other structures, such as the track, the rigidity and damping of the fasteners between the track and floating slab were consistent with the form of rail transit line 5. The specific parameters are as follows.

The train speed was $v = 60\,\mathrm{km/h}$, the track irregularity spectrum was selected as the American class-6 random irregularity, a heavy rail was used for track with a linear density of $60\,\mathrm{kg/m}$, the elastic modulus of rail was $E_\mathrm{r} = 2.1 \times 10^{11}\,\mathrm{Pa}$, the cross-sectional area of the rail was $A_\mathrm{r} = 7.708 \times 10^{-3}\,\mathrm{m}^2$, the moment of inertia of the rail was $I_\mathrm{r} = 3.203 \times 10^{-5}\,\mathrm{m}^4$, the rigidity and damping of the fasteners and plates between the track and

floating slab were 4.5×10^7 N/m and $8.433\,3 \times 10^5$ N·s/m, respectively, the lineic mass of the floating slab was 1 500 kg/m, and the stiffness between floating slab (0.6 m unit length) and viaduct was 4.5×10^{11} N/m with zero damping. The viaduct was a simply supported girder. In the numerical simulation, the time step was set to 0.5 ms, and the lineic mass of rail was 60 kg/m with a length of 46.4 m.

Using these parameters, the measured dynamic responses of the train body and those obtained using the VSDAP are shown in Figs. 5(a) and 5(b), respectively. The vertical acceleration vibration peaks in the two figures represent the vibration responses of the rail at the position where the four pairs of wheels under the two axles of the corresponding single carriage passed over the viaduct span. The distances between the axles and wheels and the train speed used in the program were consistent with the measured values, so the interval between its peak values should also be the same. To reduce the number of calculations, only one carriage was used in the calculation. The comparison shows that the calculated peak value and interval between the peak values were very close to the measured values, which validated the program and model proposed in this paper.

The concept of contact loss between the wheel and rail in this paper means that the wheel and rail were in incomplete contact due to all types of contact loss, including rail corrugations, distortion, and welds. Thus, the wheel and rail may be in contact sometimes and out of contact at other times. The contact loss was modeled as a special type of rail irregularity in this study.

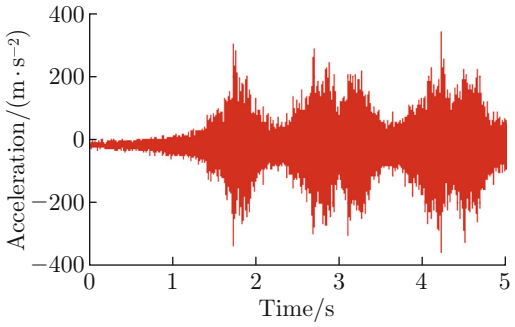

(a) Measured vertical rail vibration (v=60.0 km/h)

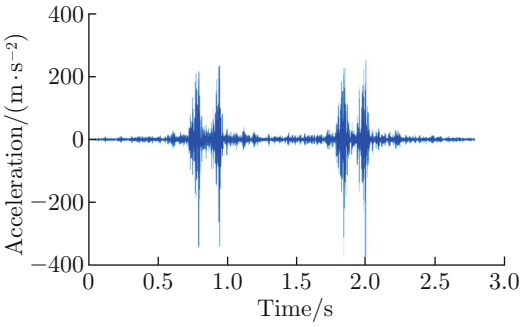

(b) Calculated vertical rail vibration (v=60.0 km/h)

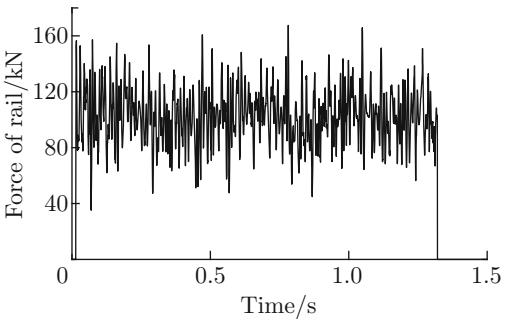

(c) Force of first wheel with no tip

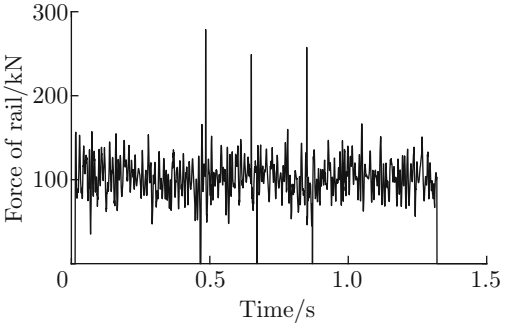

(d) Force of first wheel with a 0.2-mm tip

Fig. 5 Validation curves

Figures 5(c) and 5(d) show the contact force between the rail and wheel when the vehicle traveled on a rail with a class-4 random irregularity at a speed of 20 m/s. The contact force was zero, which meant that there was wheel-rail contact loss. This further proved the validity of the current model considering the wheel-rail contact loss.

5 Numerical Examples

Rail irregularities have the greatest impact on vehicle comfort. This example serves to illustrate the effects of the abruptness of the random irregularities on the riding comfort and to analyze the differences between the passenger and vehicle comfort.

The abruptness of the rail irregularity refers to the convexity and concavity at some parts of the rail on the operating line due to rail corrosion, severe wear, tears, sudden subsidence, or loose bearings. Based on the China Ministry of Railways Standard (TB 2097—89), the allowable wear limits and the wear geometry parameter changes of the rail are presented in Tables 2 and 3. Only a small abruptness was considered, which would not cause the other geometric parameters of the rail to change. Thus, the value range of the abruptness was ±3 mm.

Table 2 Allowed wear limits of slightly damaged rails

Lineic mass/ ($kg \cdot m^{-1}$)	Total wear/mm		Vertical wear/mm		Side wear/mm	
	Start and finish station line	Other station lines	Start and finish station line	Other station lines	Start and finish station line	Other station lines
60	14	16	9	10	14	16
50	12	14	8	9	12	14
43	10	12	7	8	10	12
38	9	10	7	8	9	11

Table 3 Sectional geometric parameter calculation data of worn rail

Lineic mass/ ($kg \cdot m^{-1}$)	Wear quantity/mm		Wear area		Moment of inertia		Moment of inertia		New center of section/mm	
	Vertical	Side	Area/mm^2	Percentage of railhead/%	I_x/cm^4	Percentage reduction/%	I_y/cm^4	Percentage reduction/%	x	y
60	3	0	107	3.7	3 092	3.9	517	1.3	0	−1.3
	6	0	288	9.9	2 938	8.7	513	2.1	0	−3.5
	7	0	349	12.0	2 886	10.3	510	2.7	0	−4.3
	8	0	419	14.4	2 828	12.1	508	3.1	0	−5.1
	9	0	483	16.6	2 772	13.8	505	3.6	0	−5.9
	10	0	558	19.2	2 712	15.7	502	4.2	0	−6.7
	12	0	705	24.3	2 589	19.5	496	5.3	0	−8.5
	14	0	828	28.5	2 485	22.8	491	6.3	0	−10.3
	16	0	897	30.9	2 428	24.5	485	7.4	0	−11.2

To investigate the effect of the abruptness on the vehicle-body and equivalent human-body interactions, four classes of abruptness: 0, 0.2 mm, 0.7 mm, and 1.2 mm based on a class-4 random irregularity, were considered. Each of the four abruptness cases was set at the peak, valley, and middle position of the class-4 random irregularity. The trigonometric series method was used to simulate the class-4 track irregularity and rail abruptness, as shown in Fig. 6[8,12,29-31].

To simplify the calculation, only one carriage was considered. The parameters of the 13-DOF model for the numerical simulation are summarized in Table 4. These parameters were similar to the values of the high-speed train and human bodies[12-13]. The parameters of the substructure were obtained from a previous report[28].

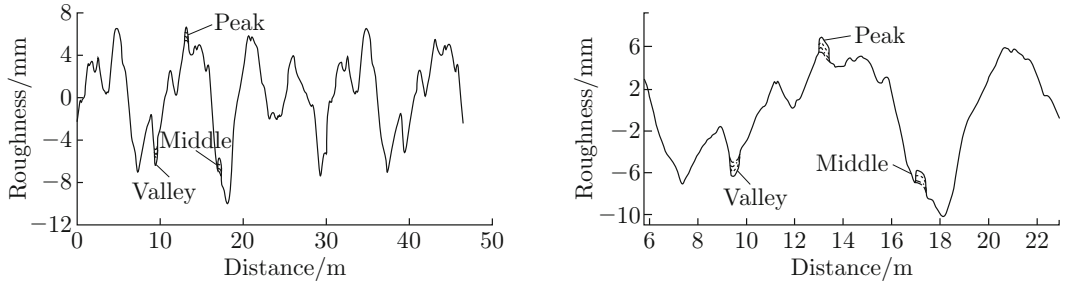

(a) Master drawing (b) Partial enlarged detail

—— FRA class-4 + 1.2 mm, ····· FRA class-4 + 0.7 mm, −·− FRA class-4 + 0.2 mm, - - - FRA class-4

Fig. 6 Profiles of four classes of track abruptness

5.1 Vibration Displacements

Figure 7 compares the vertical displacements at four different points, including the vehicle-body, front-coupling-point, middle-coupling-point, and rear-coupling-point under the four different abruptness values. In addition, the average values and variances of the vertical vibration displacement at four different locations under four different abruptness values are

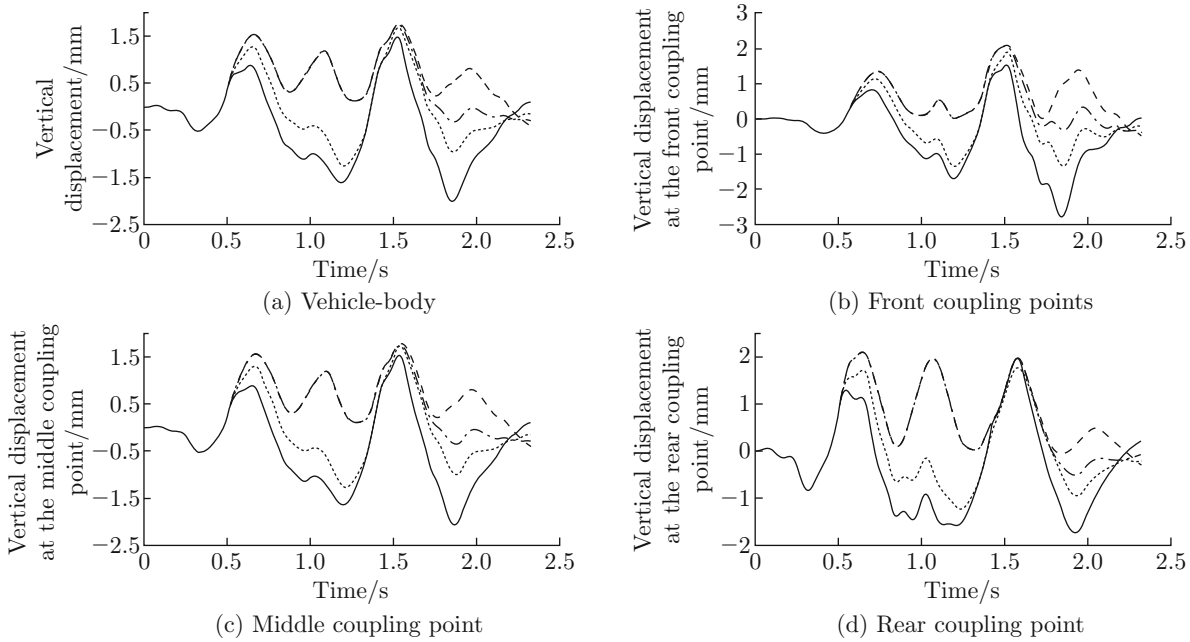

(a) Vehicle-body (b) Front coupling points

(c) Middle coupling point (d) Rear coupling point

Fig. 7 Vertical vibration displacements of the vehicle and three passengers with four different rail abruptness values (v = 20 m/s)

Table 4 Parameters of vehicle and passengers

Parameter	Value
Mass of passengers/kg	75
Mass of vehicle/t	3.2
Mass of bogie/t	3.04
Mass of wheel/t	1.0
Stiffness of primary suspension system/ $(\mathrm{kN \cdot m^{-1}})$	1 180
Stiffness of secondary suspension system/ $(\mathrm{kN \cdot m^{-1}})$	530
Stiffness between passengers and vehicle/ $(\mathrm{kN \cdot m^{-1}})$	660
Damping of primary suspension system/ $(\mathrm{kN \cdot s \cdot m^{-1}})$	39.2
Damping of secondary suspension system/ $(\mathrm{kN \cdot s \cdot m^{-1}})$	90.2
Damping between passengers and vehicle/ $(\mathrm{kN \cdot s \cdot m^{-1}})$	19.8
Distance between centers of gravity of bogies/m	17.5
Distance between two wheels under the same bogie/m	2.5
Length of the vehicle/m	20

Note: the number of passengers is 33.

Table 5 Average value of vertical vibration displacement 10^{-4} m

Location	0-mm abruptness	0.2-mm abruptness	0.7-mm abruptness	1.2-mm abruptness
Vehicle body	−3.96	−2.97	−1.55	0.97
Front passenger	4.74	2.99	−0.95	−4.45
Middle passenger	5.178 5	3.788 8	−0.523 5	−3.851 2
Rear passenger	5.613 5	4.589 7	−9.556 4	−3.248 2

Table 6 Variance of vertical vibration displacement 10^{-7} m^2

Location	0-mm abruptness	0.2-m abruptness	0.7-mm abruptness	1.2-mm abruptness
Vehicle body	3.459 9	4.023 2	4.960 9	6.897 2
Front passenger	4.182 8	4.081 1	5.376 7	8.492 1
Middle passenger	3.582 7	4.196 8	5.262 3	7.287 8
Rear passenger	5.792 6	6.718 8	7.118 6	9.368 2

summarized in Tables 5 and 6.

Figure 7(a) shows the vertical vibration displacements of the vehicle body at a speed of 20 m/s. The vibration responses of the vehicle body caused by the 0.2-mm, 0.7-mm, and 1.2-mm abruptness values were 16.28%, 43.38%, and 99.22% larger than that caused by 0-mm abruptness, respectively.

Figure 7(b) shows the vertical vibration displacements of the front equivalent passengers at a speed of

20 m/s. The vibration responses caused by 0.2-mm, 0.7-mm, and 1.2-mm abruptness values were 2.43%, 28.54%, and 103.02% larger than that caused by the 0-mm abruptness, respectively.

Figure 7(c) shows the vertical vibration displacements of the middle equivalent passengers at a speed of 20 m/s. The vibration responses of the middle equivalent passenger caused by 0.2-mm, 0.7-mm, and 1.2-mm abruptness values were 17.14%, 46.88%, and 103.41% larger than that caused by 0-mm abruptness, respectively.

Figure 7(d) shows the vertical vibration displacements of the rear equivalent passengers at a speed of 20 m/s. The vibration responses of the rear equivalent passenger caused by the 0.2-mm, 0.7-mm, and 1.2-mm abruptness values were 15.99%, 22.89%, and 61.73% larger than that caused by the 0-mm abruptness, respectively.

The results reveal that as the rail abruptness increased, the amplitude of the vibrational displacement of the vehicle body and three equivalent passenger bodies also increased, while the equivalent rear passenger location was the slowest growing point. As shown in Fig. 7, the largest amplitude of the vertical vibration displacements was 3 mm at the front equivalent passenger location, and the second largest was 2.5 mm at the rear equivalent passenger. Both amplitudes of the vehicle body and the middle equivalent passenger were 2 mm. The vertical vibration acceleration at four positions are analyzed in the next section.

5.2 Vibration Accelerations

The train speed was again set to 20 m/s^2. Figure 8 compares the vertical vibration accelerations at four different points, including the vehicle body, front-coupling point, middle-coupling point, and rear-coupling point for the four different abruptness values. The largest amplitude of the vertical vibration acceleration was 0.8 m/s^2 at the equivalent front passenger location, and the second largest was 0.6 m/s^2 at the rear equivalent passenger location. Both amplitudes of the vehicle body and the middle equivalent passenger were 0.4 m/s^2. These results are consistent with results in Ref. [13], which further verified the conclusions on the vertical vibration displacement in the previous section.

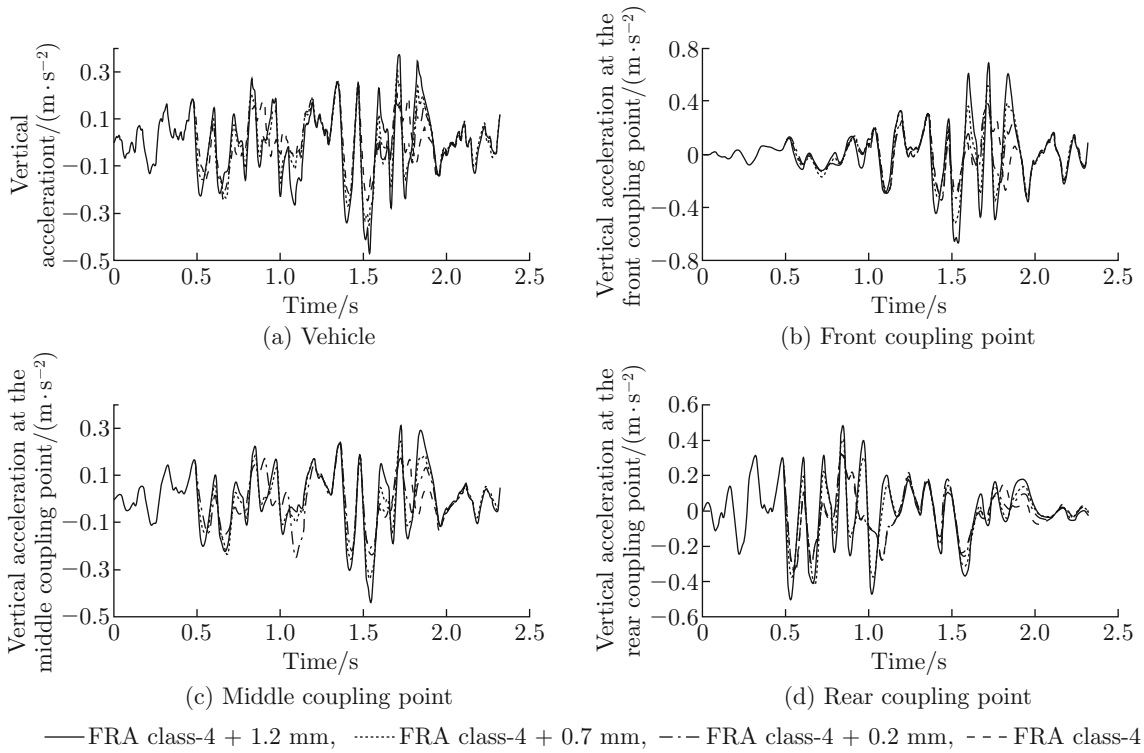

Fig. 8 Vibration acceleration responses of the vehicle and three passengers with four classes rail abruptness

The train riding comfort is a very important parameter for high-speed vehicles, and the vertical acceleration of the vehicle has a great impact on the riding comfort of the train. The human-train interaction vibrations for four different rail abruptness values and at different speeds from 0 to 90 m/s with 5 m/s increments were calculated using a custom Fortran program. The results are shown in Figs. 9—12.

Figure 11 shows that only the maximum vertical acceleration at the middle equivalent passenger under the four kinds of abruptness conditions all met the standard of 0.49 m/s^2, which is an intuitive result.

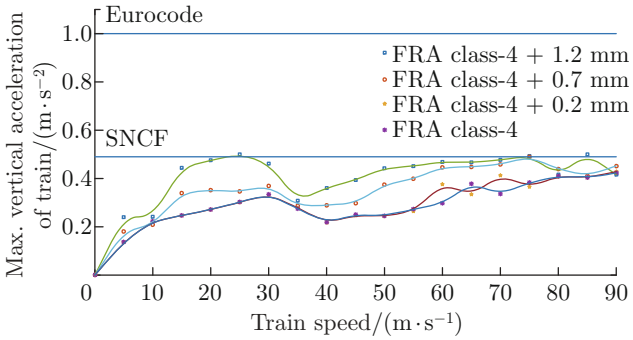

Fig. 9 Maximum vertical acceleration of vehicle body

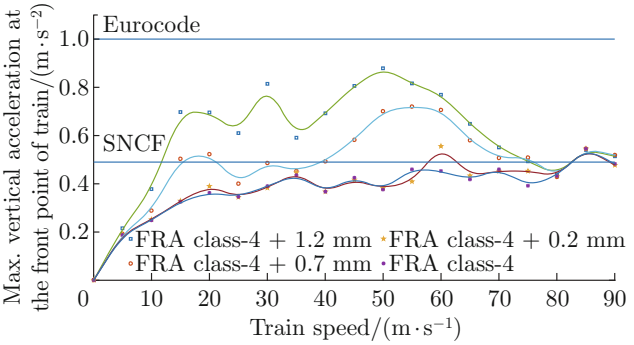

Fig. 10 Maximum vertical acceleration of front equivalent passenger

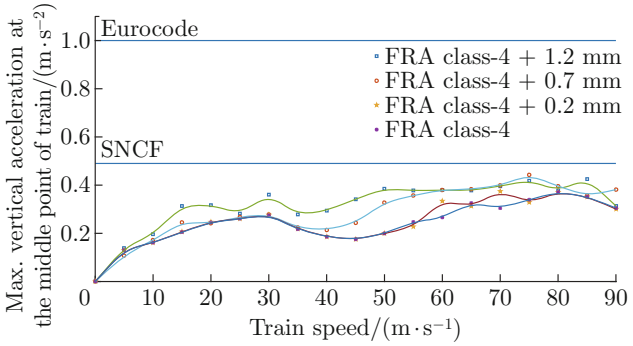

Fig. 11 Maximum vertical acceleration of middle equivalent passenger

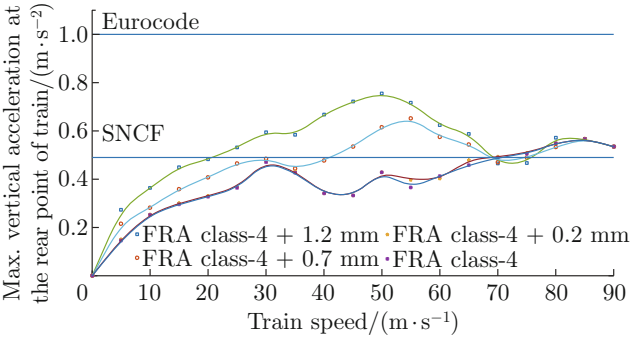

Fig. 12 Maximum vertical acceleration of rear equivalent passenger

As shown in Figs. 9, 10, and 12, the impacts of the irregularity on the front passenger and rear passenger were reduced considerably when the train speed was over 80 m/s and 70 m/s, respectively. Thus, the common-sense notion that a larger irregularity would create greater discomfort for the passenger may not be accurate. To analyze the optimal train comfort approach more clearly, Fig. 13 compares the maximum

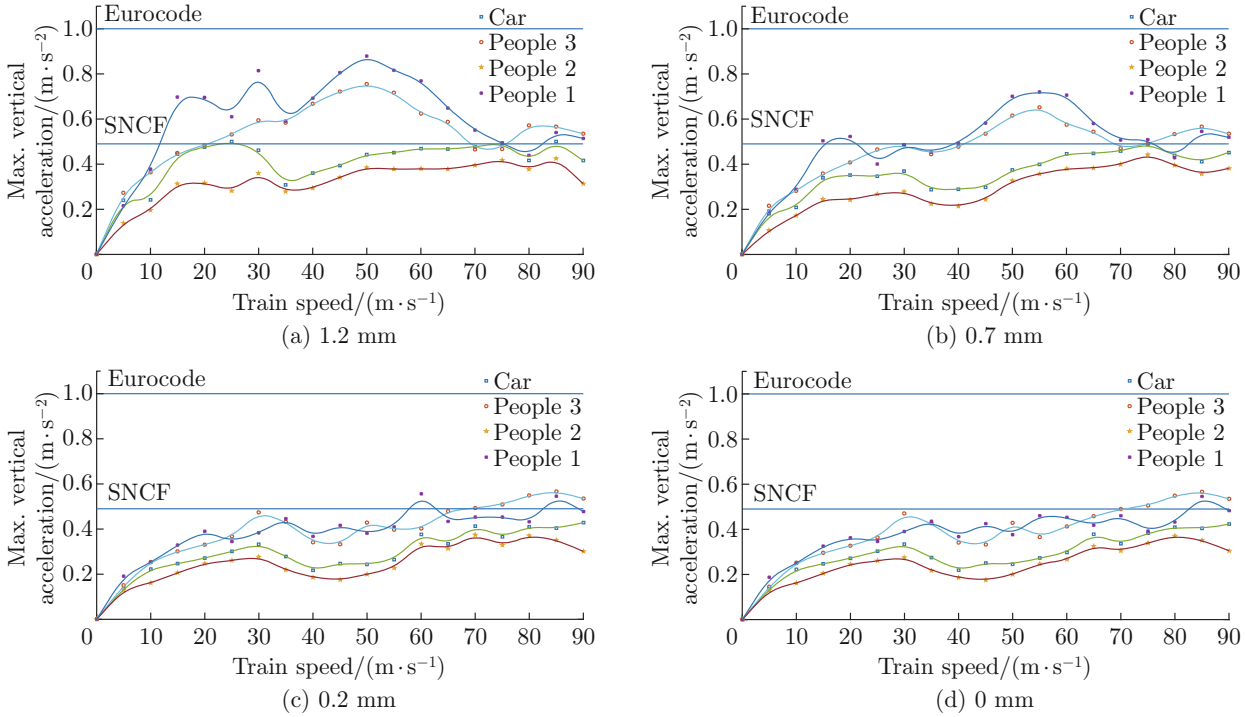

Fig. 13 Maximum vertical acceleration in four positions with abruptness values

vertical accelerations under four different abruptness values of 0, 0.2 mm, 0.7 mm, and 1.2 mm at four different locations.

Figure 13(a) shows that the vibration acceleration of the front passenger was larger than that of the rear passenger within the speed range of 10—75 m/s, and this was opposite within the speed range of 75—90 m/s when the rail abruptness was 1.2 mm. Furthermore, Figs. 13(b)—13(d) all show the same tendency, where the front passenger's vibration acceleration was larger than the rear passenger's vibration acceleration within the range of 10—25 m/s and vice versa within the range of 25—35 m/s. However, as shown in Fig. 13(b), the front passenger's vibration acceleration was higher than the rear passenger's vibration acceleration within the range of 35—75 m/s and vice versa in the range of 75—90 m/s when the rail abruptness was 0.7 mm.

The phenomena shown in Figs. 13(c) and 13(d) were more complex. The front passenger's acceleration was higher than that of the rear passenger in the range of 35—65 m/s except for a speed of 50 m/s, at which this result was reversed. When the speed was in the range of 65—90 m/s, the rear passenger's acceleration was higher than the front passenger's acceleration. Thus, the best data for the train comfort calculation were not obtained from the train body but from the dynamic passenger positions.

In summary, the traditional method of calculating the maximum vertical acceleration of the vehicle body to estimate riding comfort is a relatively conservative method, which can no longer satisfy the increasing demand for train comfort. The largest vibration and the location of worst comfort in the carriage are the best available data for train comfort evaluation. Therefore, when the dynamic largest vibration response is used as an index for comfort calculations, the comfort of the entire coach will be optimal.

6 Conclusion

Based on the classical 10-DOF vehicle and Euler beam interaction model, a bigger passenger-vehicle-line-viaduct coupling model was built and verified through a comparison with field measurements and simulation results. Numerical analysis was utilized to analyze the dynamic responses of the vehicle and three equivalent humans. Furthermore, differences between the comfort and equivalent passenger comfort were discussed. The main conclusions are as follows.

(1) A bigger and more complete passenger-vehicle-line-viaduct interaction model was built and verified by the close agreement between the simulated results and the field measured data. Relative to the separate passenger-train model, the separate rail-bridge model, or the vehicle-Euler beam model, this model is not only more realistic but also easier to use in simulations because every model parameter can be changed easily, and the effect on each part of this model (including passengers, train body, rail, bridge, rail, floating slab, and bridge) can be captured.

(2) Only the rail irregularity spectrum is input, and the model automatically judges when and where the wheel-rail contact or wheel-rail separation occurs. This feature is closer to the actual operation of a train.

(3) To determine the comfort of the train, instead of considering the train body, different passenger locations should be considered, which will vary as the train passes track irregularities. All of the previous train vertical Sperling index standards were based on vehicle body vibrations. However, with the rapid development of high-speed rail and the increasing requirements for riding comfort of the passengers, the traditional comfort standard is gradually becoming less effective. The model in this paper indicates that considering the vibrations of the equivalent passengers is more realistic and suitable for meeting the high comfort standards.

Appendix A: Generalized Stiffness Matrix

$$\boldsymbol{C}_{\mathrm{v}} = \begin{bmatrix}
3C_{\mathrm{p}}+2C_{\mathrm{z2}} & 0 & -C_{\mathrm{z2}} & 0 & -C_{\mathrm{z2}} & 0 & 0 & 0 & 0 & 0 & -C_{\mathrm{p1}} & -C_{\mathrm{p2}} & -C_{\mathrm{p3}} \\
0 & 2C_{\mathrm{z2}}l_{\mathrm{c}}^2+2C_{\mathrm{p}}l_{\mathrm{c}}^2 & -C_{\mathrm{z2}}l_{\mathrm{c}} & 0 & C_{\mathrm{z2}}l_{\mathrm{c}} & 0 & 0 & 0 & 0 & 0 & -C_{\mathrm{p1}}l_{\mathrm{c}} & 0 & C_{\mathrm{p3}}l_{\mathrm{c}} \\
-C_{\mathrm{z2}} & -C_{\mathrm{z2}}l_{\mathrm{c}} & 2C_{\mathrm{z1}}+C_{\mathrm{z2}} & 0 & 0 & 0 & -C_{\mathrm{z1}} & -C_{\mathrm{z1}} & 0 & 0 & 0 & 0 & 0 \\
0 & 0 & 0 & 2l_{\mathrm{t}}^2C_{\mathrm{z1}} & 0 & 0 & -l_{\mathrm{t}}C_{\mathrm{z1}} & l_{\mathrm{t}}C_{\mathrm{z1}} & 0 & 0 & 0 & 0 & 0 \\
-C_{\mathrm{z2}} & C_{\mathrm{z2}}l_{\mathrm{c}} & 0 & 0 & 2C_{\mathrm{1z}}+C_{\mathrm{z2}} & 0 & 0 & 0 & -C_{\mathrm{z1}} & -C_{\mathrm{z1}} & 0 & 0 & 0 \\
0 & 0 & 0 & 0 & 0 & 2l_{\mathrm{t}}^2C_{\mathrm{z1}} & 0 & 0 & -l_{\mathrm{t}}C_{\mathrm{z1}} & l_{\mathrm{t}}C_{\mathrm{z1}} & 0 & 0 & 0 \\
0 & 0 & -C_{\mathrm{z1}} & -l_{\mathrm{t}}C_{\mathrm{z1}} & 0 & 0 & C_{\mathrm{z1}} & 0 & 0 & 0 & 0 & 0 & 0 \\
0 & 0 & -C_{\mathrm{z1}} & l_{\mathrm{t}}C_{\mathrm{z1}} & 0 & 0 & 0 & C_{\mathrm{z1}} & 0 & 0 & 0 & 0 & 0 \\
0 & 0 & 0 & 0 & -C_{\mathrm{z1}} & -l_{\mathrm{t}}C_{\mathrm{z1}} & 0 & 0 & C_{\mathrm{z1}} & 0 & 0 & 0 & 0 \\
0 & 0 & 0 & 0 & -C_{\mathrm{z1}} & l_{\mathrm{t}}C_{\mathrm{z1}} & 0 & 0 & 0 & C_{\mathrm{z1}} & 0 & 0 & 0 \\
-C_{\mathrm{p1}} & C_{\mathrm{p1}}l_{\mathrm{c}} & 0 & 0 & 0 & 0 & 0 & 0 & 0 & 0 & C_{\mathrm{p1}} & 0 & 0 \\
-C_{\mathrm{p2}} & 0 & 0 & 0 & 0 & 0 & 0 & 0 & 0 & 0 & 0 & C_{\mathrm{p2}} & 0 \\
-C_{\mathrm{p3}} & -C_{\mathrm{p3}}l_{\mathrm{c}} & 0 & 0 & 0 & 0 & 0 & 0 & 0 & 0 & 0 & 0 & C_{\mathrm{p3}}
\end{bmatrix}_{13\times13},$$

$$\boldsymbol{K}_{\mathrm{v}}=\begin{bmatrix}
3K_{\mathrm{p}}+2K_{\mathrm{z2}} & 0 & -K_{\mathrm{z2}} & 0 & -K_{\mathrm{z2}} & 0 & 0 & 0 & 0 & 0 & -K_{\mathrm{p1}} & -K_{\mathrm{p2}} & -K_{\mathrm{p3}} \\
0 & 2K_{\mathrm{z2}}l_{\mathrm{c}}^2-2K_{\mathrm{p}}l_{\mathrm{c}}^2 & -K_{\mathrm{z2}}l_{\mathrm{c}} & 0 & K_{\mathrm{z2}}l_{\mathrm{c}} & 0 & 0 & 0 & 0 & 0 & -K_{\mathrm{p1}}l_{\mathrm{c}} & 0 & K_{\mathrm{p3}}l_{\mathrm{c}} \\
-K_{\mathrm{z2}} & -K_{\mathrm{z2}}l_{\mathrm{c}} & 2K_{\mathrm{z1}}+K_{\mathrm{z2}} & 0 & 0 & 0 & -K_{\mathrm{z1}} & -K_{\mathrm{z1}} & 0 & 0 & 0 & 0 & 0 \\
0 & 0 & 0 & 2l_{\mathrm{t}}^2K_{\mathrm{z1}} & 0 & 0 & -l_{\mathrm{t}}K_{\mathrm{z1}} & l_{\mathrm{t}}K_{\mathrm{z1}} & 0 & 0 & 0 & 0 & 0 \\
-K_{\mathrm{z2}} & K_{\mathrm{z2}}l_{\mathrm{c}} & 0 & 0 & 2K_{\mathrm{z1}}+K_{\mathrm{z2}} & 0 & 0 & 0 & -K_{\mathrm{z1}} & -K_{\mathrm{z1}} & 0 & 0 & 0 \\
0 & 0 & 0 & 0 & 0 & 2l_{\mathrm{t}}^2K_{\mathrm{z1}} & 0 & 0 & -l_{\mathrm{t}}K_{\mathrm{z1}} & l_{\mathrm{t}}K_{\mathrm{z1}} & 0 & 0 & 0 \\
0 & 0 & -K_{\mathrm{z1}} & -l_{\mathrm{t}}K_{\mathrm{z1}} & 0 & 0 & K_{\mathrm{z1}} & 0 & 0 & 0 & 0 & 0 & 0 \\
0 & 0 & -K_{\mathrm{z1}} & l_{\mathrm{t}}K_{\mathrm{z1}} & 0 & 0 & 0 & K_{\mathrm{z1}} & 0 & 0 & 0 & 0 & 0 \\
0 & 0 & 0 & 0 & -K_{\mathrm{z1}} & -l_{\mathrm{t}}K_{\mathrm{z1}} & 0 & 0 & K_{\mathrm{z1}} & 0 & 0 & 0 & 0 \\
0 & 0 & 0 & 0 & -K_{\mathrm{z1}} & l_{\mathrm{t}}K_{\mathrm{z1}} & 0 & 0 & 0 & K_{\mathrm{z1}} & 0 & 0 & 0 \\
-K_{\mathrm{p1}} & K_{\mathrm{p1}}l_{\mathrm{c}} & 0 & 0 & 0 & 0 & 0 & 0 & 0 & 0 & K_{\mathrm{p1}} & 0 & 0 \\
-K_{\mathrm{p2}} & 0 & 0 & 0 & 0 & 0 & 0 & 0 & 0 & 0 & 0 & K_{\mathrm{p2}} & 0 \\
-K_{\mathrm{p3}} & -K_{\mathrm{p3}}l_{\mathrm{c}} & 0 & 0 & 0 & 0 & 0 & 0 & 0 & 0 & 0 & 0 & K_{\mathrm{p3}}
\end{bmatrix}_{13\times 13},$$

where l_{t} is half of the distance between two suspension centers above the bogie.

Appendix B: Vehicle passing line-bridge structure

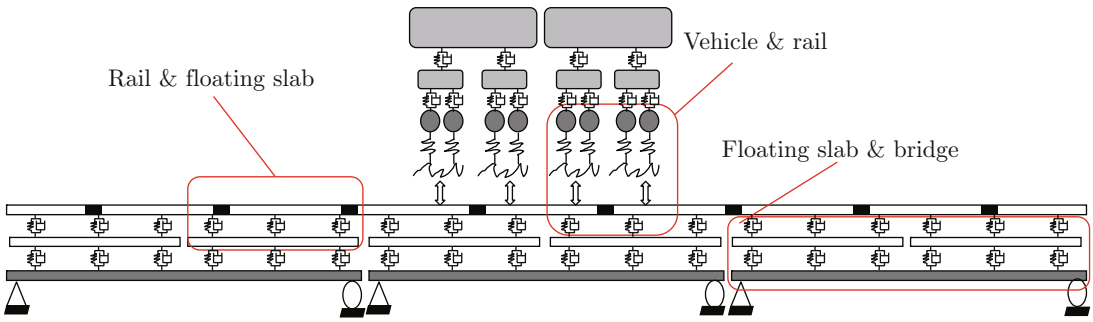

The vibration equations and parameters of the track and viaduct model can be found in Appendix B of the author's previous paper[23].

References

[1] ROMÁN C, MARTÍN J C. Integration of HSR and air transport: Understanding passengers' preferences [J]. *Transportation Research Part E*: *Logistics and Transportation Review*, 2014, **71**: 129-141.

[2] ZHAI W M, ZHAO C F, XIA H, et al. Basic scientific issues on dynamic performance evolution of the high-speed railway infrastructure and its service safety [J]. *Scientia Sinica* (*Technologica*), 2014, **44**(7): 645-660 (in Chinese).

[3] YANG Y B, YAU J D, HSU L C. Vibration of simple beams due to trains moving at high speeds [J]. *Engineering Structures*, 1997, **19**(11): 936-944.

[4] YAU J D, WU Y S, YANG Y B. Impact response of bridges with elastic bearings to moving loads [J]. *Journal of Sound and Vibration*, 2001, **248**(1): 9-30.

[5] FRÝBA L. A rough assessment of railway bridges for high speed trains [J]. *Engineering Structures*, 2001, **23**(5): 548-556.

[6] XIAO F, CHEN G S, HULSEY J L, et al. Characterization of nonlinear dynamics for a highway bridge in Alaska [J]. *Journal of Vibration Engineering & Technologies*, 2018, **6**(5): 379-386.

[7] HUNG C F, HSU W L. Influence of long-wavelength track irregularities on the motion of a high-speed train [J]. *Vehicle System Dynamics*, 2018, **56**(1): 95-112.

[8] LING L, ZHANG Q, XIAO X B, et al. Integration of car-body flexibility into train-track coupling system dynamics analysis [J]. *Vehicle System Dynamics*, 2018, **56**(4): 485-505.

[9] CUTINI M, BRAMBILLA M, BISAGLIA C. Assessment of a ride comfort number for agricultural tractors: A simplified approach [J]. *Biosystems Engineering*, 2019, **185**: 35-44.

[10] CHANG K C, WU F B, YANG Y B. Disk model for wheels moving over highway bridges with rough surfaces [J]. *Journal of Sound and Vibration*, 2011, **330**(20): 4930-4944.

[11] DENG L, CAI C S. Identification of parameters of vehicles moving on bridges [J]. *Engineering Structures*, 2009, **31**(10): 2474-2485.

[12] RAMALINGAM M, DAVIDSON JEBASEELAN D. The effect of vibration characteristics of an automotive seating system on ride comfort: A finite element

study [J]. *Proceedings of the Institution of Mechanical Engineers, Part C: Journal of Mechanical Engineering Science*, 2019, **233**(18): 6588-6601.

[13] JIANG P B, LING L, DING X, et al. Track irregularity sensitive wavelengths of high-speed railway considering flexible vibration of vehicle body [J]. *Journal of Vibration and Shock*, 2021, **40**(15): 79-89.

[14] YOUCEF K, SABIHA T, MOSTAFA D, et al. Dynamic analysis of train-bridge system and riding comfort of trains with rail irregularities [J]. *Journal of Mechanical Science and Technology*, 2013, **27**(4): 951-962.

[15] TOMIOKA T, TAKIGAMI T, SUZUKI Y. Numerical analysis of three-dimensional flexural vibration of railway vehicle car body [J]. *Vehicle System Dynamics*, 2006, **44**(sup1): 272-285.

[16] TOMIOKA T, TAKIGAMI T. Experimental and numerical study on the effect due to passengers on flexural vibrations in railway vehicle carbodies [J]. *Journal of Sound and Vibration*, 2015, **343**: 1-19.

[17] TOMIOKA T, TAKIGAMI T, AIDA K. Experimental investigations on the damping effect due to passengers on flexural vibrations of railway vehicle carbody and basic studies on the mimicry of the effect with simple substitutions [J]. *Vehicle System Dynamics*, 2017, **55**(7): 995-1011.

[18] HUI C, WEIHUA Z, MIAO B R. Vertical vibration analysis of the flexible carbody of high speed train [J]. *International Journal of Vehicle Structures and Systems*, 2015, **7**(2): 55-60.

[19] GONG D, ZHOU J S, SUN W J. Passive control of railway vehicle car body flexural vibration by means of underframe dampers [J]. *Journal of Mechanical Science and Technology*, 2017, **31**(2): 555-564.

[20] DUMITRIU M. On the critical points of vertical vibration in a railway vehicle [J]. *Archive of Mechanical Engineering*, 2014, **61**(4): 609-625.

[21] DUMITRIU M. A new passive approach to reducing the carbody vertical bending vibration of railway vehicles [J]. *Vehicle System Dynamics*, 2017, **55**(11): 1787-1806.

[22] CHEN R, CHEN J Y, WANG P, et al. Impact of wheel profile evolution on wheel-rail dynamic interaction and surface initiated rolling contact fatigue in turnouts [J]. *Wear*, 2019, **438/439**: 203109.

[23] LIU X W, XIE J, WU C, et al. Semi-analytical solution of vehicle-bridge interaction on transient jump of wheel [J]. *Engineering Structures*, 2008, **30**(9): 2401-2412.

[24] YANG Y B, YAU J D, WU Y S. Vehicle-bridge interaction dynamics - with applications to high-speed railways [M]. Singapore: World Scientific Publishing Co. Pte. Ltd., 2004.

[25] MADSHUS C, KAYNIA A M. High-speed railway lines on soft ground: Dynamic behaviour at critical train speed [J]. *Journal of Sound and Vibration*, 2000, **231**(3): 689-701.

[26] HIRT M A. Eurocode 1: Basis of design and actions on structures [J]. *Schweizer Ingenieur und Architekt*, 1993(16/17): 273-275.

[27] LEBEL D, SOIZE C, FÜNFSCHILLING C, et al. Statistical inverse identification for nonlinear train dynamics using a surrogate model in a Bayesian framework [J]. *Journal of Sound and Vibration*, 2019, **458**: 158-176.

[28] WU C, LIU X W, HUANG X C. Alterable-element method for vehicle-bridge interaction considering the transient jump of wheel [J]. *Journal of Shanghai Jiaotong University* (*Science*), 2008, **13**(3): 330-335.

[29] PERRIN G, DUHAMEL D, SOIZE C, et al. Quantification of the influence of the track geometry variability on the train dynamics [J]. *Mechanical Systems and Signal Processing*, 2015, **60/61**: 945-957.

[30] LIU X D, WANG H X, SHAN Y C, et al. Construction of road roughness in left and right wheel paths based on PSD and coherence function [J]. *Mechanical Systems and Signal Processing*, 2015, **60/61**: 668-677.

[31] XU L, ZHAI W M. A novel model for determining the amplitude-wavelength limits of track irregularities accompanied by a reliability assessment in railway vehicle-track dynamics [J]. *Mechanical Systems and Signal Processing*, 2017, **86**: 260-277.